Electrical Power and Energy Systems 152 (2023) 109236

Contents lists available at ScienceDirect

International Journal of Electrical Power and Energy Systems

journal homepage: www.elsevier.com/locate/ijepes

A Non-unit transient travelling wave protection scheme for multi-terminal HVDC system

Botong Li [a,b,*], Yuqi Li [a,b], Bin Li [a,b], Xiaolong Chen [a,b], Liang Ji [c], Qiteng Hong [d]

[a] Key Laboratory of Smart Grid of Minist of Education, Tianjin University, Tianjin 300072, China
[b] National Industry-Education Integration Platform of Energy Storage, Tianjin University, Tianjin 300072, China
[c] Department of Electronic and Electrical Engineering, University of Strathclyde, Glasgow G1 1XQ, UK
[d] Department of Electrical Power Engineering, Shanghai University of Electric Power, Shanghai 200090, China

ARTICLE INFO

Keywords:
Multi-terminal HVDC grid
Dc line protection scheme
High speed
Non-unit

ABSTRACT

The rapid and accurate dc line protection scheme is of great value in isolating dc line faults and improving the reliability of multi-terminal HVDC systems. Nowadays, the traveling wave (TW) protection is widely used as the primary protection in HVDC transmission systems. However, the traditional TW protection has the problems of poor resistance to high impedance faults and the setting value depends on simulation. For the hybrid three-terminal LCC/MMC HVDC system, this paper provides a fast non-unit protection scheme. Firstly, the time-domain expressions of the backward line-mode voltage TW after different line faults occur are derived respectively. Based on the expressions, a non-unit protection scheme depending on the difference value of the line-mode backward TW is proposed. Finally, the scheme is verified by simulation. The method only needs single-ended data to realize the rapid dc line protection without converter station communication which has a clear theoretical calculation method in setting values and a strong robustness to high-resistance fault.

Nomenclature

TW	abbreviation for traveling wave
U_{f1}, I_{f1}	line-mode fault voltage and current at the fault point
U_{dc+}	voltage on the line L1 under the normal operation of system
R_f	fault resistance
Z_{c1}, Z_{c0}	line-mode and zero-mode wave impedance of the overhead line
B_{f1}	backward line-mode traveling wave at the fault point
k_a, k_t	attenuation and distortion coefficient of the traveling wave propagation
l_f	distance from the fault point to the measuring point
l_1	length of the overhead line L1
v	propagation velocity of the line-mode traveling wave
B_{m1}	backward line-mode fault traveling wave at the measuring point
B_{m0}	backward zero-mode fault traveling wave at the measuring point
C_{eq}	equivalent capacitance of the MMC station
L_{eq}	sum of the equivalent inductance of the MMC station and the induction of the current limiting reactor
L_r	induction of the current limiting reactor
T_s	time window for protection
t_{st}	the start-up time of the protection
Δt_0	time interval between the adjacent sampling points
u_m	volage at the measuring point
u_{m1}, i_{m1}	line-mode fault voltage and current at the measuring point
u_{m0}, i_{m0}	zero-mode fault voltage and current at the measuring point
K_{set}	threshold of the fault area identification component
D_{set}	threshold of the fault direction component
P_{ser}	threshold of the fault pole selection component
Δ_1	threshold of the start-up component

* Corresponding author at: Key Laboratory of Smart Grid of Minist of Education, Tianjin University, Tianjin 300072, China.
E-mail address: libotong@tju.edu.cn (B. Li).

https://doi.org/10.1016/j.ijepes.2023.109236
Received 22 December 2022; Received in revised form 4 March 2023; Accepted 8 May 2023
Available online 23 May 2023

1. Introduction

The hybrid three-terminal HVDC system comprises a line commutation converter (LCC) at the sending end and modular multi-level converters (MMC) at the receiving end to efficiently prevent inverter commutation failure [1–4]. Hybrid multi-terminal HVDC system offers a wide range of potential applications in distributed new energy access and multi-drop power transmission which is more cost-effective and flexible than conventional HVDC transmission techniques [5–7]. Currently, China has completed the Kun-Liu-Long hybrid three-terminal HVDC transmission project, which supported the West-East power transmission project significantly.

The long transmission distance and complex working environment make the dc overhead line (OHL) become the components with the highest failure rate in the hybrid multi-terminal HVDC system. Due to the existence of the MMC converter station, when the OHL fault occurs in the system, the fault current rises quickly. It is important to identify and cut off the fault OHL fast and accurately to ensure the safe operation and rapid recovery of the non-fault part of the system [8]. Therefore, accurate and fast protection scheme in hybrid multi-terminal HVDC system is particularly important [9].

In a hybrid multi-terminal DC system, if both ends of the dc line have boundary components such as current-limiting reactors, the difference of electrical quantity characteristics at both ends of the boundary elements can be utilized to identify the fault area. [10] proposes a method for identifying fault lines by comparing the voltage change rates at both ends of the current-limiting reactor. [11] identifies the fault line by comparing the transient voltage amplitudes at both ends of the reactor, which enhances the robustness to fault resistance and can effectively identify the fault with a 300 Ω fault resistance. However, the above method will not be applicable if there are no boundary elements at both ends of the line in the hybrid multi-terminal HVDC system. For example, the current-limiting reactor of the Kun-Liu-Long hybrid three-terminal HVDC system is located at the outlet of the converter at the middle bus, rather than at both ends of the DC line. In this case, the above method is not feasible.

For a multi-terminal HVDC transmission system, longitudinal differential approach is proposed to locate the fault line. [12] proposes the protection scheme of longitudinal differential, which can locate the fault line accurately. However, the longitudinal differential requires communication between converter stations to exchange information. In order to avoid the influence of distributed capacitive current, a time delay is required at the same time. In a hybrid multi-terminal HVDC system, the MMC converter station quickly locks or switches to a negative voltage output state after a dc line fault occurs, and the LCC converter station will also carry out forced phase shift control. The time delay will weaken the characteristics of fault electrical quantity, thus, the fault line identification method with long-time delay is no longer applicable [13]. Therefore, a hybrid multi-terminal HVDC transmission system needs a protection scheme with a higher speed.

The traveling wave (TW) approach is widely employed for dc line protection in multi-terminal HVDC system, which has the characteristics of rapid action and high sensitivity [14]. [15] identifies the fault direction by comparing the ratio of the high frequency components of the forward and backward TW which has a strong robustness to high-resistance fault. [16] proposes a protection scheme based on the integral of backward TW divided by forward TW, and the rapid dc line protection is realized. However, the TW direction criterion proposed in [15,16] are all based on the differences of TW characteristics obtained from the simulation, and meanwhile the setting value also depends on simulation. [17] proposes using the first peak time of the transient voltage after a fault occurrence to identify the fault, which demonstrates robustness to high transition resistance and acts quickly. [18] obtains the analytical time-domain expression of the electrical quantity through analytical calculation, and identified the difference in the electrical quantity between internal and external faults according to the time-domain expression. Although the method proposed in [17,18] requires further investigation under close-in faults with low sampling frequency, it offers researchers a new approach to designing novel TW protection schemes using the time-domain expression of fault TW.

In this paper, a fast non-unit TW protection scheme is proposed. The novel protection has a strong robustness to high-resistance fault and noise interference. It also has a clear theoretical calculation method in setting values. The section in this paper is organized as follows. In section 2, the time-domain expressions of the backward line-mode voltage TW at the measuring point are obtained after different line faults occur. In section 3, the TW fault characteristics are analyzed based on the time-domain expression of the backward TW and a novel non-unit TW protection scheme depending on the difference of the backward TW is proposed. The setting value calculation formula is also given based on the TW expressions. In section 4, simulation is used to validate the scheme, and the robustness test of the scheme is also validated.

2. Analysis of fault TW characteristics

This paper takes the Kun-Liu-Long hybrid three-terminal HVDC system as the research reference. Fig. 1 shows the basic structure of the system.

LCC converter station is the system feeder and the other two MMC converter stations are receivers. LCC station connects the MMC_1 station with the OHL L1. MMC_1 station connects the MMC_2 station with the OHL L2, and the OHL L1 and L2 are connected to the MMC_1 station through the confluent bus. Table 1 shows the detailed system parameters [19].

For the bipolar HVDC system, electrical coupling exists between the two poles. The phasor is converted to the modulus for decoupling, and the phase-mode transformation equation is expressed as follows:

$$\begin{bmatrix} F_0 \\ F_1 \end{bmatrix} = \frac{1}{\sqrt{2}} \begin{bmatrix} 1 & 1 \\ 1 & -1 \end{bmatrix} \begin{bmatrix} F_p \\ F_n \end{bmatrix} \tag{1}$$

where F represents the electrical quantity, and the subscripts 0, 1 represent the zero-mode and line-mode components respectively; the subscripts p and n denote positive pole quantities and negative pole

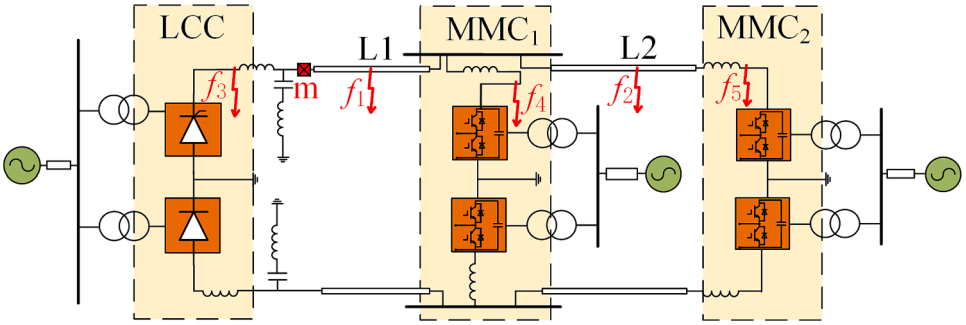

Fig. 1. The topology of hybrid three-terminal DC system.

Table 1
Parameters of system.

Parameter	Value
Length of L1, L2(km)	908,542
Rated DC voltage(kV)	800
Rated power of LCC, MMC_1, MMC_2(MVA)	9720,3132,5100
Outlet inductance of LCC(H)	0.15
Outlet inductance of MMC(H)	0.075
Bridge arm inductance of MMC (H)	0.1
Submodule capacitance of MMC (F)	0.015

quantities respectively.

There exist line-mode components after faults occur for both pole-to-pole(P-P) and pole-to-ground(P-G) faults, and the attenuation and distortion of the line-mode components in the OHL are relatively small. Therefore, this study utilizes the line-mode components for the fault line identification. Within several hundred microseconds after the fault occurs, the system control link does not play a significant role, so the influence of the control link can be ignored, and the system can be approximately regarded as a linear system. In order not to be affected by the load component, according to the superposition theorem of the linear system, this paper only analyzes the fault component.

The location of the fault point (f_1, f_2, f_3, f_4, f_5) and measuring point (m) is shown in Fig. 1. The time-domain expressions of the backward fault TW B_{m1} at the measuring point m when the fault occurs at different positions in the system are obtained respectively.

2.1. Analysis of the TW B_{m1} in case of f_1 fault

The fault point f_1 is located on the OHL L1. It can be considered that the fault point sends out fault TW B_f. B_f directly propagates to the measuring point m through the OHL L1.

According to [20], the line-mode fault voltage U_{f1} at the fault point when pole-to-ground(P-G) and pole-to-pole(P-P) fault occurs on L1 can be obtained as:

$$U_{f1} = \begin{cases} \dfrac{-U_{dc+}Z_{c1}}{R_f + Z_{c1}} & \text{P - P fault} \\ \dfrac{-U_{dc+}Z_{c1}}{Z_{c1} + Z_{c0} + 4R_f} & \text{P - G fault} \end{cases} \tag{2}$$

where U_{dc+} is the voltage on L1 under the normal operation of system, R_f is the fault resistance, Z_{c1} and Z_{c0} are the line-mode and ground-mode wave impedance of the OHL respectively.

The expression of U_{f1} in the s domain can be obtained as:

$$U_{f1}(s) = \begin{cases} \dfrac{-U_{dc+}Z_{c1}}{R_f + Z_{c1}}\dfrac{1}{s} & \text{P - P fault} \\ \dfrac{-U_{dc+}Z_{c1}}{Z_{c1} + Z_{c0} + 4R_f}\dfrac{1}{s} & \text{P - G fault} \end{cases} \tag{3}$$

The expression of the backward fault TW B_{f1} can be obtained as:

$$B_{f1}(s) = U_{f1}(s) - Z_{c1}I_{f1}(s) = 2U_{f1}(s) \tag{4}$$

TW will attenuate and distort in the process of propagation. (5) is used to approximate the distortion effect of the OHL on TW [21]. k_a is the attenuation coefficient of TW, k_t is the distortion coefficient of TW, and l_f is the distance from the fault point to the measuring point m.

$$A_1(s) = \frac{1 - k_a l_f}{1 + s k_t l_f} \tag{5}$$

The TW B_{m1} can be expressed as:

$$B_{m1}(s) = B_{f1}(s)A_1(s) \tag{6}$$

The time-domain expression of the TW B_{m1} can be obtained by performing the *Inverse Laplace Transform* on (6), which can be expressed as:

$$B_{m1}(t) = 2U_{f1}(1 - k_a l)(1 - e^{\frac{-1}{k_t l_f}t}) \tag{7}$$

2.2. Analysis of the TW B_{m1} in case of f_2 fault

The fault TW sent by the fault point f_2 will first pass through the bus and then propagate to the measuring point m when the fault occurs on the OHL L2. The TW propagation diagram is shown in Fig. 2.

The TW B_{f1} at the fault point f_2 propagates to the bus through the OHL L2 firstly, and then refracts at the bus. The equivalent circuit diagram can be obtained when the TW refracts at the bus, as shown in Fig. 3. In the figure, C_{eq} is the equivalent capacitance of the MMC station, L_{eq} is the sum of the equivalent inductance of the MMC station and the inductance of the current limiting reactor at the outlet of the MMC station [22].

According to Fig. 3, the expression of the TW B_{m1} can be obtained when the TW B_{f1} at the fault point refracts at the bus and then propagates to the measurement point m. The expression is shown as:

$$B_{m1}(s) = B_{f1}(s)\frac{1 - k_a l_f}{1 + s k_t l_f}\left[1 - \frac{Z_{c1}}{2L_{eq}\left(s + \frac{Z_{c1}}{2L_{eq}}\right)}\right] \tag{8}$$

The time-domain expression of the TW B_{m1} can be obtained by performing the *Inverse Laplace Transform* on (8), which can be expressed as:

$$B_{m1}(t) = 2U_{f1}(1 - k_a l_f)\left(e^{\frac{-Z_{c1}}{2L_{eq}}t} - e^{\frac{-1}{k_t l_f}t}\right) \tag{9}$$

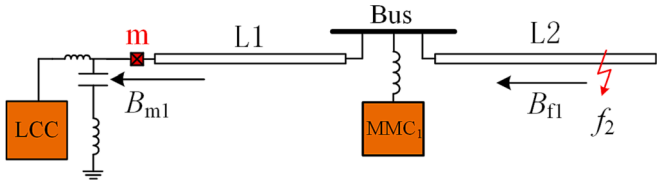

Fig. 2. TW propagation diagram in case of f_2 fault.

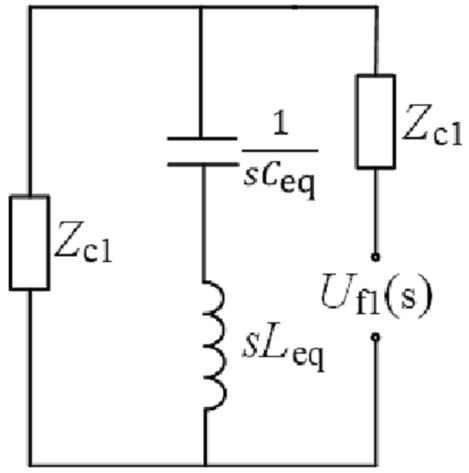

Fig. 3. The equivalent circuit diagram of TW refraction at the confluent bus.

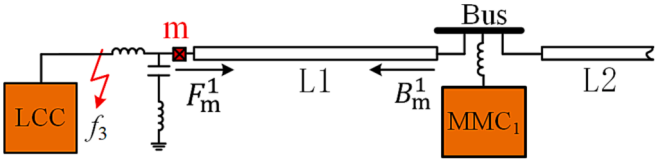

Fig. 4. TW propagation diagram in case of f_3 fault.

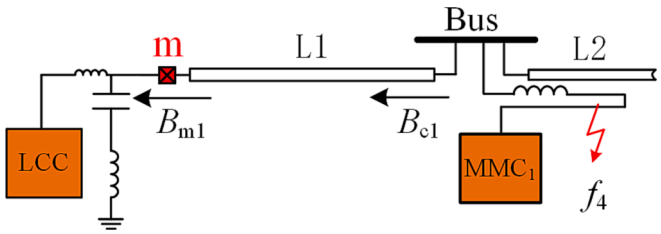

Fig. 5. TW propagation diagram in case of f_4 fault.

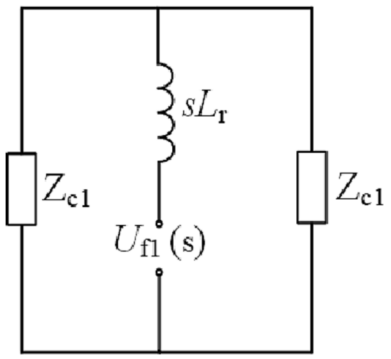

Fig. 6. The equivalent circuit diagram at the fault point f_4.

2.3. Analysis of the TW B_{m1} in case of f_3 fault

The fault point f_3 is located at the outlet of LCC converter station, and the transmission process of the fault TW is shown in Fig. 4. The fault point f_3 sends out the forward fault TW F_m^1 at time t_0. The TW F_m^1 propagates to the bus and then reflects at the bus, forming the backward fault TW B_m^1.

The backward fault TW cannot be detected at the measuring point m before the backward fault TW B_m^1 reaches the measuring point m. Therefore, the expression of the backward fault TW B_{m1} can be obtained as:

$$B_{m1}(t) = 0 \ (t_0 \le t \le t_0 + \frac{2l_1}{v}) \tag{10}$$

where l_1 is the length of the OHL L1, and v is the propagation velocity of the line-mode TW.

2.4. Analysis of the TW B_{m1} in case of f_4 fault

The fault TW B_{c1} is generated at the end of the OHL L1 when fault occurs at the fault point f_4, and then propagates to the measuring point m through the OHL L1. The TW propagation diagram is shown in Fig. 5.

The fault point f_4 is located at the outlet of the converter station MMC_1, and the equivalent circuit diagram at the fault point is shown in Fig. 6. In the figure, L_r is the inductance of current limiting reactor at the outlet of the converter station MMC_1.

According to Fig. 6, the expression of fault TW B_{c1} at the end of the OHL L1 can be obtained as:

$$B_{c1}(s) = \frac{U_{f1}Z_{c1}}{L_r s(s + \frac{Z_{c1}}{2L_r})} \tag{11}$$

The TW B_{c1} propagates through the OHL L1 and arrives at the measuring point m forming the backward TW B_{m1}. The expression of the TW B_{m1} can be obtained as:

$$B_{m1}(s) = B_{c1}(s)\frac{1 - k_a l_f}{1 + s k_t l_f} = \frac{U_{f1}Z_{c1}(1 - k_a l_f)}{L_r s(s + \frac{Z_{c1}}{2L_r})(1 + s k_t l_f)} \tag{12}$$

According to the data in Table 1 and the OHL parameters, the following relations can be obtained.

$$L_r >> k_t l_f Z_{c1} \tag{13}$$

According to (13), the expression of the TW B_{m1} can be simplified as:

$$B_{m1}(s) = 2U_{f1}(1 - k_a l_f)(1 - \frac{1}{s + \frac{Z_{c1}}{2L_r}}) \tag{14}$$

The time-domain expression of the TW B_{m1} can be obtained as (15) by performing the *Inverse Laplace Transform* on (14).

$$B_{m1}(t) = 2U_{f1}(1 - k_a l_f)(1 - e^{-\frac{Z_{c1}}{2L_r}t}) \tag{15}$$

2.5. Analysis of the TW B_{m1} in case of f_5 fault

The fault point f_5 is located at the outlet of the converter station MMC_2. After the fault occurs, the TW B_{c2} is formed at the end of the OHL L2. The TW B_{c2} firstly refracts at the bus through the OHL L2, and then propagates to the point m forming the backward TW B_{m1}. The TW propagation diagram is shown in Fig. 7.

The equivalent circuit diagram at the fault point f_5 is shown as Fig. 8.

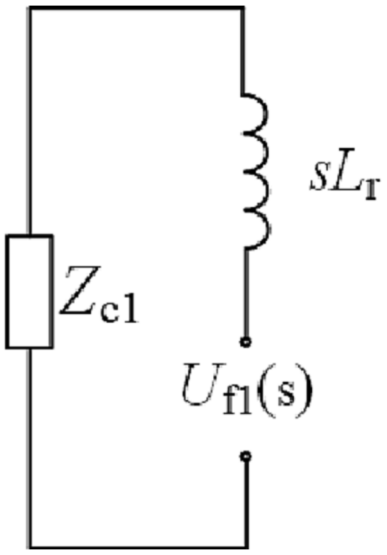

Fig. 8. The equivalent circuit diagram at the fault point f_5.

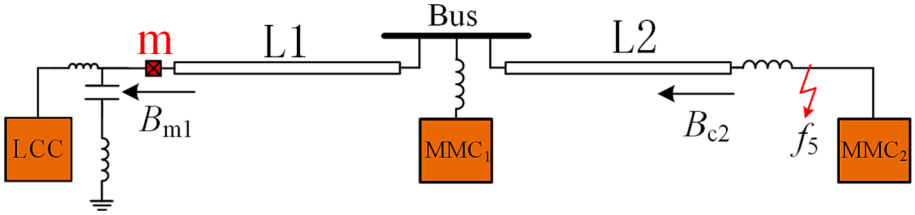

Fig. 7. TW propagation diagram in case of f_5 fault.

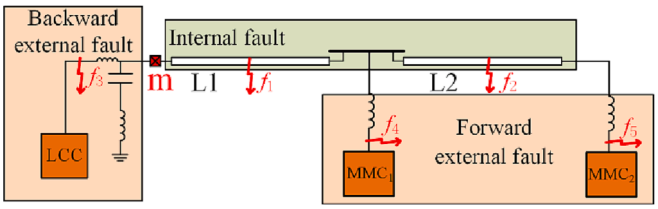

Fig. 9. The specific protection scope.

According to the Fig. 8, the expression of the backward TW B_{c2} can be obtained as:

$$B_{c2}(s) = \frac{2U_{f1}Z_{c1}}{L_r s(s+\frac{Z_{c1}}{L_r})} \tag{16}$$

The TW B_{c2} refracts at the bus and then propagates to the measuring point m forming the backward TW B_{m1}. According to (8) and (16), the expression of B_{m1} can be obtained as:

$$B_{m1}(s) = \frac{1-k_a l}{1+sk_t l}\frac{2U_f Z_{c1}}{L_r s(s+\frac{Z_{c1}}{L_r})}[1-\frac{Z_{c1}}{2L_{eq}(s+\frac{Z_{c1}}{2L_{eq}})}] \tag{17}$$

According to (13), the expression of B_{m1} can be simplified as:

$$B_{m1}(s) = \frac{4U_{f1}L_{eq}}{2L_{eq}-L_r}(\frac{1}{s+\frac{Z_{c1}}{2L_{eq}}}-\frac{1}{s+\frac{Z_{c1}}{L_r}}) \tag{18}$$

The time-domain expression of the TW B_{m1} can be obtained as (19) by performing the *Inverse Laplace Transform* on (18).

$$B_{m1}(t) = \frac{4U_{f1}L_{eq}}{2L_{eq}-L_r}(e^{-\frac{Z_{c1}}{2L_{eq}}t}-e^{-\frac{Z_{c1}}{L_r}t}) \tag{19}$$

3. A Non-Unit TW protection scheme

In multi-terminal HVDC system, a complete non-unit protection scheme mainly includes start-up, fault area identification and fault pole selection component. There are relatively mature methods for start-up and fault pole selection component. This paper focuses on the construction of a novel fault area identification component.

For the Kun-Liu-Long hybrid three-terminal HVDC system, when a fault occurs at any position in the DC line area (L_1, L_2), the LCC converter station must quickly identify the fault and shift the phase to clear the fault current. Therefore, the protection range of the TW protection at m covers all DC lines (L_1, L_2). The specific protection range is shown in Fig. 9.

3.1. Start-up component

In this paper, the difference value of the voltage is taken as the characteristic quantity of the start-up component. When the difference value is greater than the threshold, the start-up component acts. The criterion is shown as:

$$\left|\frac{dU_m}{dt}\right| > \Delta_1 \tag{20}$$

U_m is the voltage at the measuring point m, Δ_1 is the setting threshold. The threshold Δ_1 has two main requirements: firstly, to ensure that the start-up component operates under any fault condition, and secondly, to ensure that it does not operate during normal system operation. The sensitivity of the start-up component is of utmost importance. In this paper, the start-up criterion threshold Δ_1 is chosen as 1.5 times the maximum voltage change rate during normal operation of the system.

3.2. Fault area identification component

Based on Fig. 9, the fault points presented in Fig. 1 can be categorized as follows: f_1 and f_2 are situated in the internal fault area, f_3 is in the backward external fault area, and f_4 and f_5 are in the forward external fault area. The parameters in Table 1 are taken into the expression of backward TW B_{m1} at different fault positions, and the results are shown in Appendix A.1. Furthermore, Fig. 10 shows the simulation and calculation waveforms of the backward TW B_{m1} under different fault points. The fault time in the simulation is set to 1.5 s, while the fault points f_1 and f_2 are located at the midpoint of OHL L1 and L2, respectively, with the fault types being metallic P-P fault and P-G fault.

Fig. 10 displays the simulation and calculation waveforms of the TW B_{m1} for the P-P fault case, as depicted in (a-1), (b-1), (c-1), (d-1), (e-1), and the TW waveforms for the P-G fault case, as illustrated in (a-2), (b-2), (c-2), (d-2), (e-2). The figure shows that the simulation waveform is essentially in agreement with the calculation waveform, which confirms the accuracy of the analytical expression of TW B_{m1}.

The simulation waveform of the TW B_{m1} starts recording at 0.5 ms before the fault TW reaches the point m, and the total recording duration is 1.5 ms. According to the TW waveform, when the fault occurs at f_1, the TW B_{m1} drops rapidly and then remains approximately constant. When the fault occurs at f_2, the TW B_{m1} drops rapidly and then starts to rise. When the fault occurs at f_3, the TW B_{m1} is approximately 0. When the fault occurs at f_4, the TW B_{m1} drops monotonically. When the fault occurs at f_5, the TW B_{m1} drops slowly and then starts to rises.

According to the above TW trend analysis and the simulation waveform, there exists a certain period T_s that the TW B_{m1} drops monotonically in the case of forward external faults (f_4 and f_5) within T_s, while the TW B_{m1} does not show a monotonically declining trend in the case of internal faults (f_1 and f_2) within T_s. Therefore, it is possible to detect whether the TW B_{m1} drops monotonically in the time period T_s to distinguish the internal and external faults. Moreover, the difference value of the TW B_{m1} can reflect the TW trend. If the difference value of the TW is always less than zero within T_s, it will be judged as forward external fault.

For the determination of the time window T_s, it is necessary to ensure that the TW B_{m1} first decreases and then rises in the case of f_2 fault within T_s, while decreasing monotonically in the case of f_5 fault. Using the time-domain expression of the TW B_{m1} obtained in Section 2, the transition time when the TW B_{m1} changes from descending to ascending can be calculated. This is done by finding the time when the first derivative of the time-domain expression is zero. For the fault occurring on f_2, the simplified expression of the transition time can be obtained as (21) based on the B_{m1} expression (9).

$$t_{f2} = k_t l_f \ln\frac{2L_{eq}}{k_t l_f Z_{c1}} \tag{21}$$

For the fault occurs on f_5, the transition time can be expressed as (22) based on the B_{m1} expression (19).

$$t_{f5} = \frac{2L_r L_{eq}}{(2L_{eq}-L_r)Z_{c1}}\ln\frac{2L_{eq}}{L_r} \tag{22}$$

Based on (21), t_{f2} is influenced by the equivalent inductance (L_{eq}), fault distance (l_f), TW distortion coefficient (k_t), and line-mode wave impedance (Z_{c1}). Deriving from (21), t_{f2} has a positive correlation with L_{eq}, l_f, k_t and a negative correlation with Z_{c1}. This means that the maximum value of t_{f2} is achieved when L_{eq}, l_f, k_t are at their highest values and Z_{c1} is at its minimum value. For a multi-terminal HVDC transmission project, the maximum equivalent inductance (L_{eq}) can be set to 0.35H, the maximum fault distance (l_f) to 1500 km, the maximum TW distortion coefficient (k_t) to 2e-8, and the minimum line-mode wave impedance (Z_{c1}) to 100 Ω. Based on these parameters, the maximum value of t_{f2} can be calculated to be 0.16 ms.

Based on (22), t_{f5} is influenced by the equivalent inductance (L_{eq}), current-limiting reactor inductance (L_r), and line-mode wave impedance

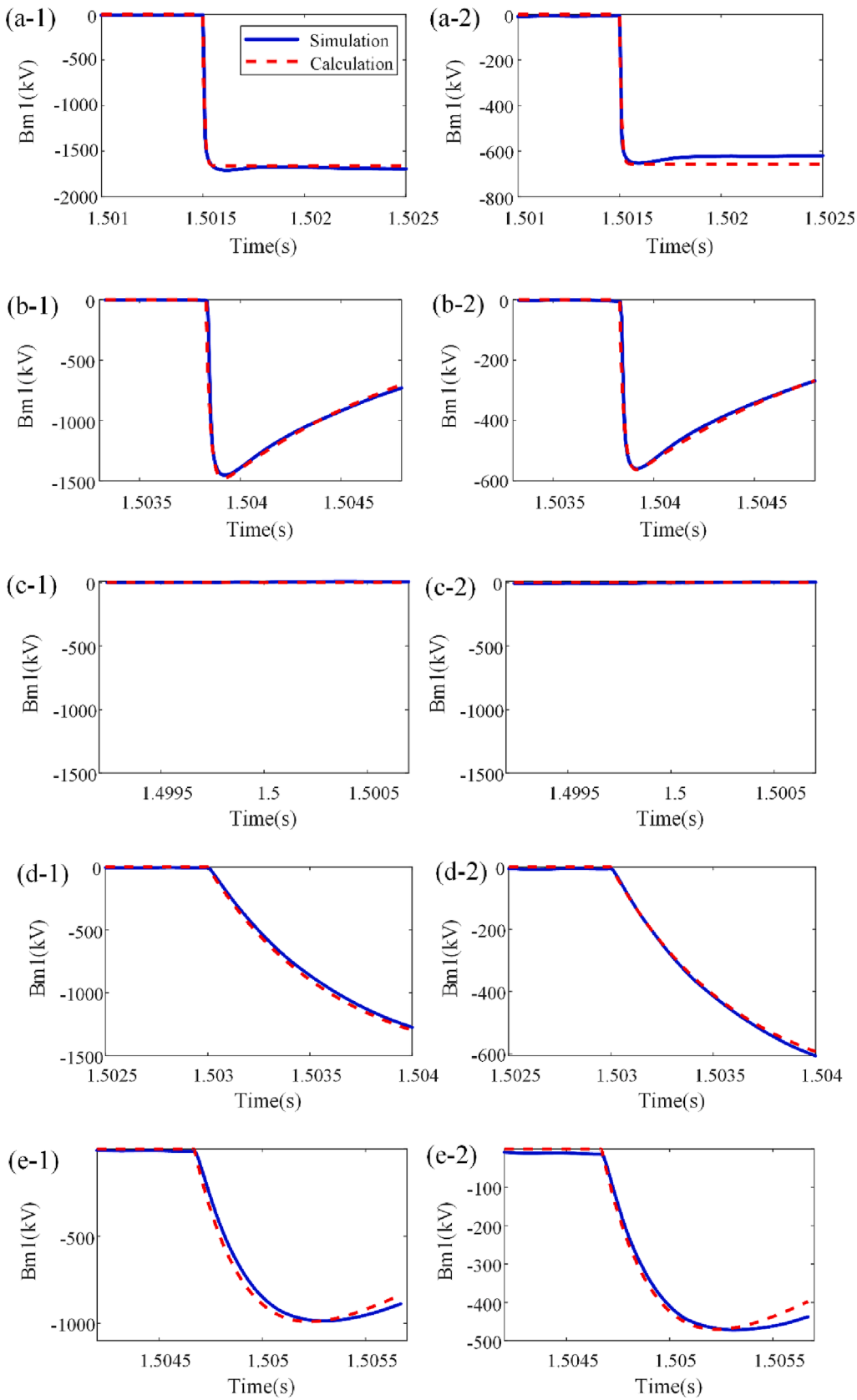

Fig. 10. The simulation and calculation waveform of the TW B_{m1} (a) internal fault occurs at f_1; (b) internal fault occurs at f_2; (c) backward external fault occurs at f_3; (d) forward external fault occurs at f_4; (e) forward external fault occurs at f_5.

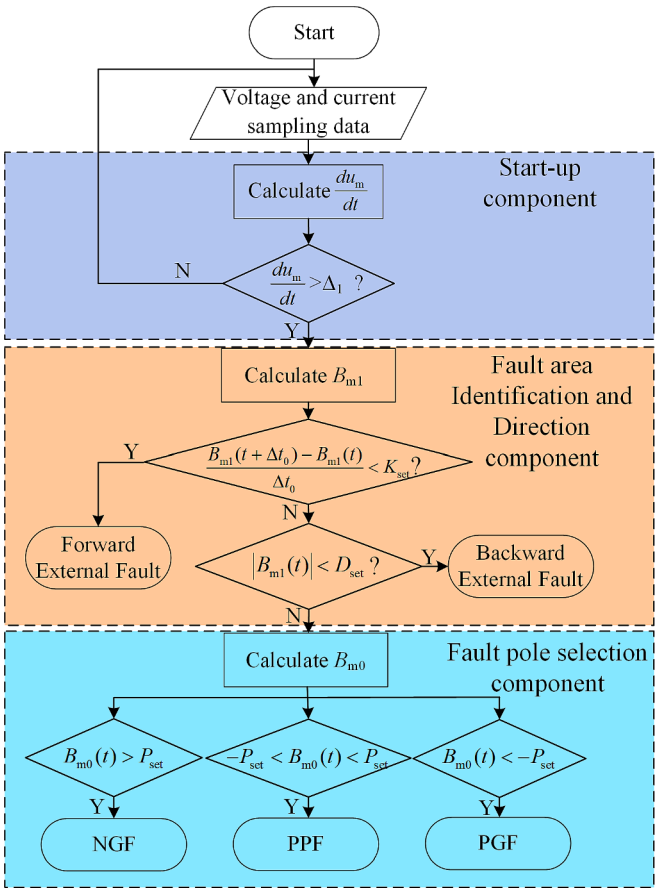

Fig. 11. The flow chart of the non-unit TW protection scheme.

(Z_{c1}). Based on the actual parameters of the HVDC transmission project, the equivalent inductance L_{eq} ranges from 0.2H to 0.35H, the current-limiting reactor inductance L_r ranges from 0.05H to 0.15H, and the maximum line-mode wave impedance is 600 Ω. Using the above information, the minimum value of t_{f5} can be calculated to be approximately 0.37 ms by traversal search.

According to the analysis above, the maximum value of t_{f2} is generally less than 0.3 ms, while the minimum value of t_{f5} is greater than 0.3 ms. Therefore, the time window T_s is set as 0.3 ms in this paper which is suitable for most HVDC transmission systems.

When a fault occurs at f_1, the TW B_{m1} drops rapidly and then remains approximately constant. During this time, noise interference can cause the waveform of TW B_{m1} to jitter easily. Therefore, to avoid misjudgment due to noise interference, a threshold K_{set} is set. If the difference value of the TW B_{m1} is always less than K_{set} within T_s, it is judged as a forward external fault. The criterion expression is shown as (23), where t_{st} is the start-up time of the protection and Δt_0 is the time interval between the sampling points. The start-up time is considered to be the time when the fault TW just reaches the measuring point m.

$$\begin{cases} \dfrac{B_{m1}(t+\Delta t_0)-B_{m1}(t)}{\Delta t_0} < K_{set} \\ t \in [t_{st}, t_{st} + T_s] \end{cases} \tag{23}$$

The TW B_{m1} can be calculated through the line-mode fault voltage u_{m1} and fault current i_{m1} at the point m, and it can be expressed as:

$$B_{m1}(t) = u_{m1}(t) - Z_{c1} i_{m1}(t) \tag{24}$$

The threshold K_{set} is calculated based on the time-domain expression of the TW B_{m1} in Section 2. K_{set} shall be selected as the maximum difference value of the TW B_{m1} in case of forward external fault (f_4 and f_5) within T_s. The second derivative of (15) and (19) of the TW B_{m1} expressions can be calculated when the fault occurs at f_4 and f_5. It can be obtained that the second derivative of the TW B_{m1} expression is always greater than zero within T_s. Therefore, the maximum difference value of the TW B_{m1} should be obtained at the last moment within T_s. The maximum difference value of the TW B_{m1} within T_s can be expressed as:

$$\max\left(\frac{dB_{m1}}{dt}\right) = \frac{B_{m1}(T_s) - B_{m1}(T_s - \Delta t_0)}{\Delta t_0} \tag{25}$$

According to (25), the maximum difference value of the TW B_{m1} when the fault occurs at f_4 and f_5 can be calculated respectively. It can be obtained that the difference value in case of f_4 fault is greater than the f_5 fault. Therefore, the threshold K_{set} should be selected as the maximum difference value of the TW B_{m1} in case of a P-G fault with a transition resistance of 500 Ω at f_4. According to (15) and (25), K_{set} can be expressed as:

$$K_{set} = 0.5\max\left(\frac{dB_{m1}}{dt}\right) = \frac{U_{f1}(1-k_a l_1)\left[e^{-\frac{Z_{c1}}{2L_r}(T_s-\Delta t_0)} - e^{-\frac{Z_{c1}}{2L_r}T_s}\right]}{\Delta t_0} \tag{26}$$

3.3. Direction component

Based on the fault analysis in Section 2.3, when a backward fault occurs, the TW B_{m1} always measures 0 within the sampling time window (T_s). Therefore, for backward faults, the modified discriminant formula for the fault direction component is shown in (27). The threshold D_{set} is chosen as 1.5 times the amplitude of maximum backward line-mode fault TW B_{m1} generated during normal operation of the system.

$$|B_{m1}(t)| \langle D_{set} \ (t_{st} \le t \le t_{st} + T_s) \tag{27}$$

3.4. Fault pole selection component

The zero-mode fault TW exists in the OHL in case of P-G fault, and the polarity of the zero-mode TW is related to the fault pole. The zero-mode TW does not exist in the OHL in case of P-P fault. Therefore, the fault pole can be identified based on the backward zero-mode fault TW B_{m0}, and the expression of the TW B_{m0} is shown as (28). u_{m0} and i_{m0} are the zero-mode fault voltage and current at the measuring point m.

$$B_{m0}(t) = u_{m0}(t) - Z_{c0} i_{m0}(t) \tag{28}$$

The criterion for the fault pole selection component is expressed as (29), and the threshold P_{set} is chosen as 1.5 times the maximum backward zero-mode fault TW B_{m0} during normal operation of the system.

$$\begin{cases} B_{m0}(t) < -P_{set} \text{ Positive P - G fault} \\ B_{m0}(t) > P_{set} \text{ Negative P - G fault} \\ -P_{set} < B_{m0}(t) < P_{set} \text{ P - P fault} \\ t_{st} \le t \le t_{st} + T_s \end{cases} \tag{29}$$

3.5. Non-unit protection scheme based on the backward TW

According to the above contents in Section 3, a complete non-unit TW protection scheme at the measuring point m can be proposed. After the start-up component acts, the internal and external faults are judged according to the fault area identification component and direction component. Finally, the fault pole is identified by the fault pole selection component. The flow chart of the protection scheme is shown as Fig. 11.

4. Simulation verification

The simulation model of the hybrid three-terminal HVDC system has been built using PSCAD/EMTDC, and its parameters are based on those of the Kun-Liu-Long hybrid three-terminal HVDC system, as shown in Table 1. The fault time has been set as 1.5 s, and the sampling frequency of the protection device has been set to 20 kHz.

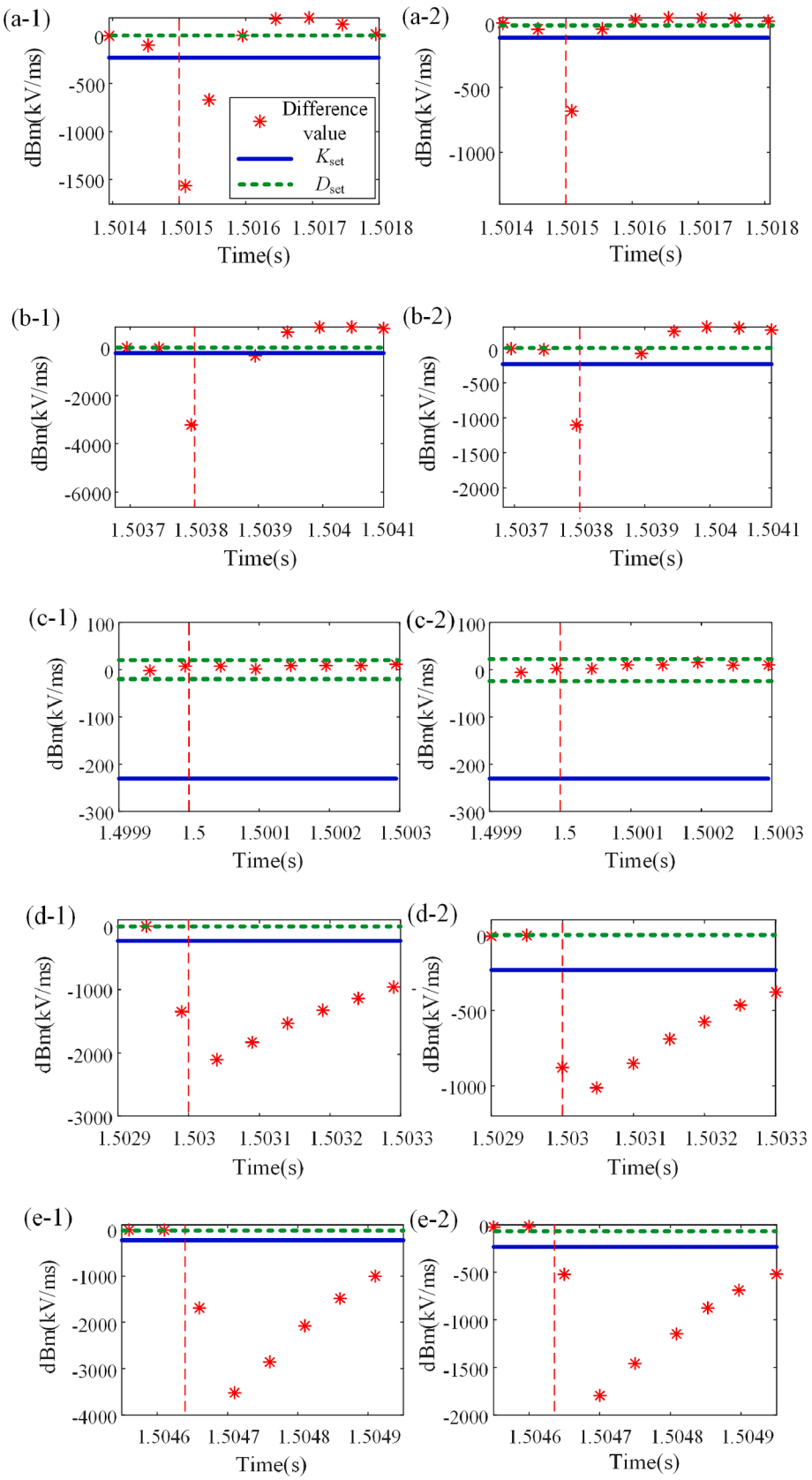

Fig. 12. Comparison of the TW difference value and threshold after faults occurs at different positions in the system (a) internal fault occurs at f_1; (b) internal fault occurs at f_2; (c) backward external fault occurs at f_3; (d) forward external fault occurs at f_4; (e) forward external fault occurs at f_5.

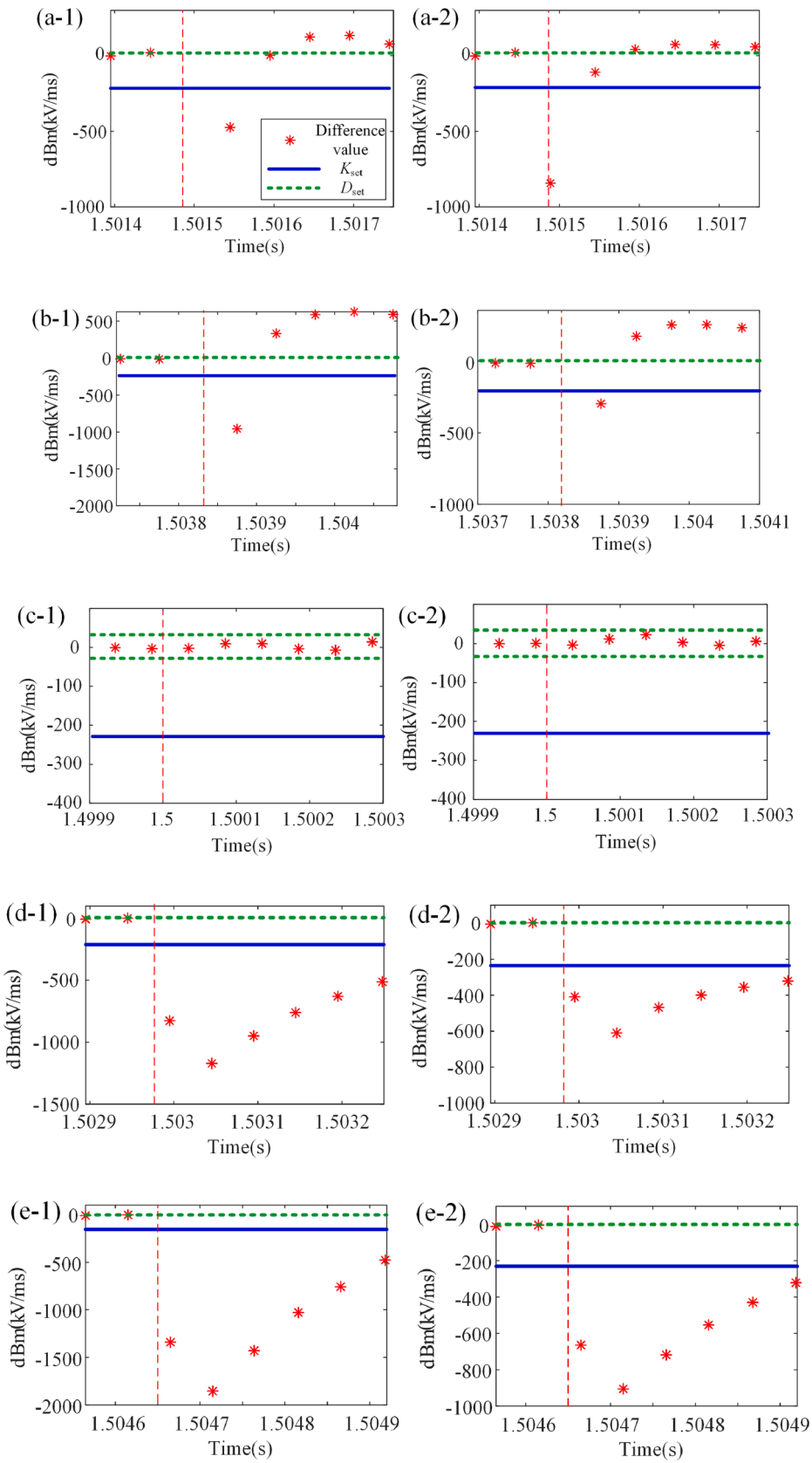

Fig. 13. Comparison of the TW difference value and threshold under 500 Ω transition resistance (a) internal fault occurs at f_1; (b) internal fault occurs at f_2; (c) backward external fault occurs at f_3; (d) forward external fault occurs at f_4; (e) forward external fault occurs at f_5.

Table 2
Robustness test of fault resistance.

Fault resistance(Ω)	Fault location	Max(dB_m/dt) (kV.ms^{-1})	Fault area	Correct operation?
100	f_1	74	Internal	√
	f_2	239	Internal	√
	f_3	9	Backward external	√
	f_4	−419	Forward external	√
	f_5	−489	Forward external	√
200	f_1	59	Internal	√
	f_2	195	Internal	√
	f_3	5	Backward external	√
	f_4	−348	Forward external	√
	f_5	−361	Forward external	√
500	f_1	38	Internal	√
	f_2	137	Internal	√
	f_3	11	Backward external	√
	f_4	−267	Forward external	√
	f_5	−281	Forward external	√

Table 3
Robustness test of noise.

SNR (dB)	Fault location	Max(dB_m/dt) (kV.ms^{-1})	Fault area	Correct operation?
15	f_1	239	Internal	√
	f_2	736	Internal	√
	f_3	45	Internal	×
	f_4	97	Internal	×
	f_5	−206	Internal	×
20	f_1	87	Internal	√
	f_2	311	Internal	√
	f_3	27	Backward external	√
	f_4	−477	Forward external	√
	f_5	−514	Forward external	√
25	f_1	65	Internal	√
	f_2	208	Internal	√
	f_3	15	Backward external	√
	f_4	−394	Forward external	√
	f_5	−370	Forward external	√

According to (26), the threshold K_{set} can be calculated as −231 kV.ms^{-1}. Through simulation testing, the threshold values for the start-up component (Δ_1), direction component (D_{set}), and fault pole selection component (P_{set}) are determined as 37 kV.ms^{-1}, 28 kV, and 25 kV, respectively. Taking into account the analysis in Section 3.2, the time window T_s is chosen to be 0.3 ms.

4.1. Verification of the fault area identification component

The fault location is illustrated in Fig. 1, where fault points f_1 and f_2 are located at the midpoint of OHL L1 and L2, respectively. The other fault points, f_3, f_4, and f_5, are situated at the outlet of the LCC, MMC_1, and MMC_2 converter stations, respectively. The fault types considered are P-G fault and P-P fault, with a transition resistance of 100 Ω. The difference value of the backward TW B_{m1} under different fault conditions is obtained and shown in Fig. 12. In the figure, the time period is

Table 4
Robustness test of sampling frequency.

Sampling-frequency (kHz)	K_{set}(kV.ms^{-1})	Fault location	Max (dB_m/dt) (kV.ms^{-1})	Fault area	Correct operation?
20	−231	f_1	207	Internal	√
		f_2	1299	Internal	√
		f_3	18	Backward external	√
		f_4	−1351	Forward external	√
		f_5	−1307	Forward external	√
50	−120	f_1	119	Internal	√
		f_2	705	Internal	√
		f_3	4	Backward external	√
		f_4	−873	Forward external	√
		f_5	−815	Forward external	√
100	−110	f_1	94	Internal	√
		f_2	689	Internal	√
		f_3	7	Backward external	√
		f_4	−749	Forward external	√
		f_5	−716	Forward external	√

Table 5
Simulation results of the Siemens TW protection.

Fault location	Fault resistance (Ω)	Δu (kV)	Fault area	Correct operation?
f_1	50	−251	Internal	√
	200	−197	External	×
f_2	50	–232	Internal	√
	200	−166	External	×
f_4	50	−73	External	√
	200	−41	External	√
f_5	50	−62	External	√
	200	−39	External	√

Table 6
Simulation results of the TW protection proposed in this paper.

Fault location	Fault resistance (Ω)	Max(dB_m/dt) (kV.ms^{-1})	Fault area	Correct operation?
f_1	50	142	Internal	√
	200	83	Internal	√
f_2	50	328	Internal	√
	200	164	Internal	√
f_4	50	−683	External	√
	200	−357	External	√
f_5	50	−764	External	√
	200	−442	External	√

from 0.1 ms before the start-up component activates and ends 0.3 ms after the start-up component has activated. The start-up time of the protection is indicated by a red dotted line.

*Fig. 12(a-1), (b-1), (c-1), (d-1), (e-1) shows the verification result in case of P-P fault, and Fig. 12(a-2), (b-2), (c-2), (d-2), (e-2) shows the verification result in case of P-G fault.

According to Fig. 12, it can be observed that for faults occurring at f_1 and f_2, the difference value of the TW B_{m1} is not consistently lower than the threshold K_{set} within T_s, and the absolute value of the difference is greater than the threshold D_{set}. Hence, it can be classified as an internal fault. For a fault occurring at f_3, the absolute value of the difference value is always lower than the threshold D_{set}, which indicates a

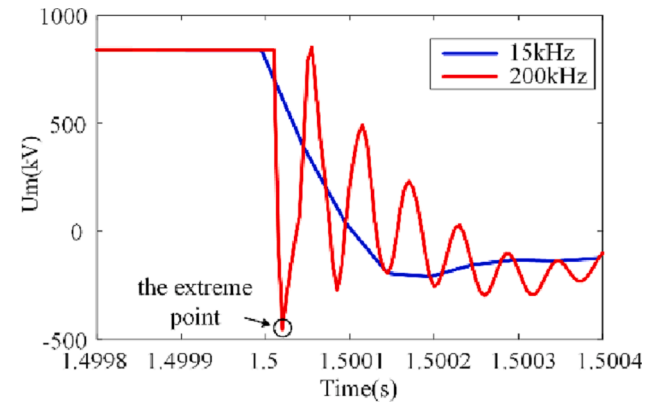

Fig. 14. The voltage waveform of different sampling frequency.

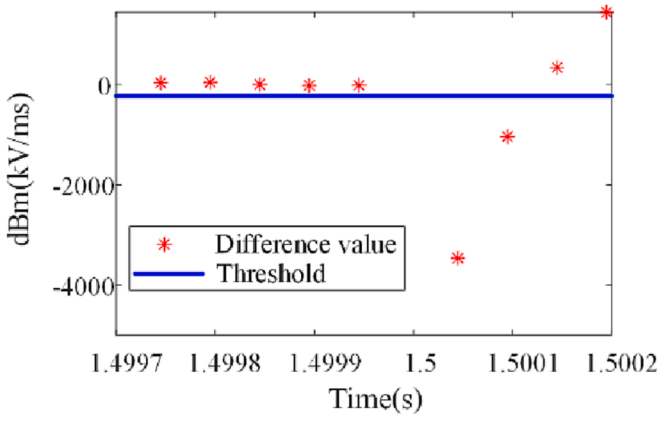

Fig. 15. Comparison of the TW difference value and threshold value.

Table A7
Time-domain expression of TW B_{m1} at different fault positions.

Fault location	P-P fault	P-G fault
f_1	$-1660*[1-e^{-123457*(t-t_t)}]$	$-656*[1-e^{-123457*(t-t_t)}]$
f_2	$-1620*[e^{-858*(t-t_t)}-e^{-48309*(t-t_t)}]$	$-616*[e^{-858*(t-t_t)}-e^{-48309*(t-t_t)}]$
f_3	0	0
f_4	$-1590*[1-e^{-1613*(t-t_t)}]$	$-740*[1-e^{-1613*(t-t_t)}]$
f_5	$-2179*[e^{-858*(t-t_t)}-e^{-3227*(t-t_t)}]$	$-1035*[e^{-858*(t-t_t)}-e^{-3227*(t-t_t)}]$

Table A8
Robustness test of fault distance.

Fault type	Fault distance (km)	Max(dB_m/dt) (kV. ms^{-1})	Fault area	Correct operation?
P-P fault	0	148	Internal	√
	200	227	Internal	√
	500	214	Internal	√
	1000	1299	Internal	√
	1400	1183	Internal	√
P-G fault	0	79	Internal	√
	200	110	Internal	√
	500	117	Internal	√
	1000	513	Internal	√
	1400	471	Internal	√

backward external fault. For faults occurring at f_4 and f_5, the difference value of the TW B_{m1} is consistently lower than the threshold K_{set} within T_s, which indicates a forward external fault. Based on the verification results, this method can accurately identify the fault location.

To further verify the method proposed in this paper, simulation tests are conducted under different parameter conditions, and the results are shown in Appendix A.2.

Table A9
Simulation verification of different value of L_r.

L_r(H)	Fault location	Max(dB_m/dt) (kV. ms^{-1})	Fault area	Correct operation?
0.05	f_2	1189	Internal	√
	f_4	−1040	Forward external	√
	f_5	−1025	Forward external	√
0.1	f_2	795	Internal	√
	f_4	−747	Forward external	√
	f_5	−726	Forward external	√
0.15	f_2	599	Internal	√
	f_4	−563	Forward external	√
	f_5	−515	Forward external	√

Table A10
Simulation verification of different value of L_{eq}.

L_{eq}(H)	Fault location	Max(dB_m/dt) (kV. ms^{-1})	Fault area	Correct operation?
0.2	f_2	895	Internal	√
	f_4	−715	Forward external	√
	f_5	−692	Forward external	√
0.25	f_2	729	Internal	√
	f_4	−714	Forward external	√
	f_5	−692	Forward external	√
0.35	f_2	438	Internal	√
	f_4	−715	Forward external	√
	f_5	−693	Forward external	√

4.2. Robustness test of transition resistance

To evaluate the effectiveness of the proposed method in handling high-resistance faults, we vary the transition resistance to 100 Ω, 200 Ω, and 500 Ω. Due to space constraints, only the graph for the difference between TW B_{m1} and the threshold value when the transition resistance is set to 500 Ω is presented in Fig. 13. Table 2 displays the maximum difference value of TW B_{m1} within T_s for different fault resistances.

According to Table 2 and Fig. 13, when the transition resistance R_f is 100 Ω, 200 Ω, and 500 Ω, the maximum difference value of B_{m1} is higher than the threshold K_{set} when the internal fault occurs. On the other hand, the maximum difference value of B_{m1} is still lower than the threshold K_{set} when the forward external fault occurs. These results demonstrate that the method proposed in this paper can accurately identify the fault area under different transition resistance conditions. The data shows that the method proposed in this paper can effectively handle the case of transition resistance of 500 Ω.

4.3. Robustness test of noise interference

To assess the ability of the proposed method to resist noise, Gaussian white noise with signal-to-noise (SNR) ratios of 15 dB, 20 dB, and 25 dB are added to TW B_{m1}. The transition resistance is set to 200 Ω, and the

fault type is P-G fault. The maximum difference value of TW B_{m1} within T_s is presented in Table 3.

Based on the data presented in Table 3, it can be observed that the proposed method accurately identifies both internal and external faults when a Gaussian white noise signal with signal-to-noise ratios of 20 dB and 25 dB is added. However, when the signal-to-noise ratio of the added Gaussian white noise signal drops to 15 dB, the fault area identification method misjudges the fault, identifying external faults as internal faults. The method proposed in this paper can correctly identify the fault when the signal-to-noise ratio of Gaussian white noise is equal to or greater than 20 dB. It is generally believed by researchers that the ability to withstand 20 dB noise is sufficient for protection devices.

4.4. Robustness test of sampling frequency

Simulations are conducted to verify the method under different sampling frequency. Set the sampling frequency at 20 kHz, 50 kHz, and 100 kHz, respectively, and test the fault identification method under different sampling frequencies. The fault type is set as metallic P-P fault, and the specific data is shown in Table 4.

According to the data in Table 4, under the condition of sampling frequency of 20 kHz, 50 kHz and 100 kHz, the method proposed in this paper can accurately identify the internal and external fault.

4.5. Comparison with other works

In order to show the superiority of the proposed method, it is compared with the traditional TW protection and a non-unit protection based on transient voltage TW respectively.

4.5.1. Comparison with the traditional TW protection

The TW protection scheme of Siemens is widely used in actual HVDC system. The TW protection scheme proposed by Siemens uses the voltage variation (Δu) to identify internal and external fault [23]. The criterion is shown as (30) for internal fault.

$$\Delta u < \Delta_{set} \tag{30}$$

According to the criterion presented in [23], the threshold Δ_{set} is determined under the condition of a P-G fault with a transition resistance of 100 Ω occurring at the end of the OHL L2. Through simulation testing, the threshold Δ_{set} is set to −229 kV. The operational performance of the Siemens TW protection and the proposed protection method under P-G faults occurring at different positions are compared and presented in Table 5 and Table 6, respectively.

It can be seen from Table 5 and Table 6 that the Siemens traditional TW protection fails when the internal fault with a transition resistance of 200 Ω occurs, while the method proposed in this paper can still accurately identify the internal and external faults in this case. It can be demonstrated that the method proposed in this paper has stronger ability to withstand high-impedance faults compared to the traditional Siemens TW protection.

4.5.2. Comparison with a non-unit protection based on transient voltage TW

Literature [18] analyzes the transient voltage TW expression when a DC line fault occurs and finds that the time of the first voltage extreme value is shorter in case of internal faults compared to external faults. The study proposes to use the time of the first voltage extreme value to distinguish between internal and external faults. This method has a strong capability to withstand high fault resistance and is characterized by high speed.

However, when the fault occurs close to the measurement point, the subsequent transient voltage waveform (TW) after the first TW arrives at the measuring point rapidly. The subsequent TW can interfere with the identification of the first voltage extreme value point and may cause the protection to fail to operate when the sampling rate is not high enough. For example, when the fault occurs 5 km away from the measuring point and the sampling frequency of the protection device is 15 kHz and 200 kHz, the voltage waveform at the measuring point can be obtained for different sampling frequencies, as shown in Fig. 14. It can be observed from Fig. 14 that the extreme point of the voltage cannot be identified when an internal fault occurs with a sampling frequency of 15 kHz, causing the protection to fail to operate.

The difference value of the TW B_{m1} can be obtained under the same fault conditions with the sampling frequency of 15 kHz, as shown in Fig. 15.

It can be seen from Fig. 15 that the difference value of the TW B_{m1} is not always less than the threshold K_{set} within T_s, which is determined as internal fault. The method proposed in this paper is still applicable. It can be demonstrated that the method proposed in this paper does not require a high sampling frequency and can accurately identifies close-in faults.

5. Conclusions

Multi-terminal hybrid LCC/MMC HVDC system is an important development direction for HVDC transmission in the future. In this paper, a non-unit protection scheme utilizing the difference value of the backward TW is proposed, and it is validated in simulation. The contributions and innovations of this paper are as follows:

- The time-domain expression of the backward TW at the measuring point after the transmission line fault is given. The formula for calculating the setting value is given based on the expression of the backward TW. The setting value does not depend on the simulation and has a clear physical meaning.
- This method only applies single-ended information, does not require inter-station communication, and has a short judgment time, which can realize rapid identification and isolation of the fault line.
- The criterion does not depend on line boundary elements and has wide applicability.

CRediT authorship contribution statement

Botong Li: Methodology, Investigation, Formal analysis, Writing – original draft. **Yuqi Li:** Data curation, Writing – original draft. **Bin Li:** Writing – review & editing. **Xiaolong Chen:** Resources, Supervision. **Liang Ji:** Writing – review & editing. **Qiteng Hong:** Resources, Supervision.

Declaration of Competing Interest

The authors declare that they have no known competing financial interests or personal relationships that could have appeared to influence the work reported in this paper.

Data availability

No data was used for the research described in the article.

Acknowledgement

The authors acknowledge the financial support from the Joint Funds of the National Natural Science Foundation of China(U2166205).

Appendix

Expression of TW B_{m1}

Table A.7

Simulation verification under different parameter conditions

Simulations are conducted to verify the method under different fault distance(l_f), with metallic P-P faults and P-G faults used as examples. The corresponding data is presented in Table A.8.

According to the information in Table A.8, the method proposed in this paper can accurately identify the DC line fault as the internal fault under different fault distance(l_f).

Simulations are conducted to verify the method under different current-limiting inductance value L_r and equivalent inductance value L_{eq}. Since the TW B_{m1} after faults f_1 and f_3 is not affected by L_r and L_{eq}, only faults f_2, f_4, and f_5 are analyzed here, with the fault type set as a metallic P-P fault. The specific data are shown in Table A.9 and A.10.

According to the data in Table A.9 and A.10, when the inductance value L_r and L_{eq} are changed, the method proposed in this paper can still correctly identify the internal and external faults.

References

[1] Zhang D, Wu C, He J, Liang C. A new protection scheme for transmission line of three-terminal hybrid HVDC system. Int J Electr Power Energy Syst 2022;134 (107446):1–10.

[2] Wang D, Cheng D, Sun X. Novel travelling wave directional pilot protection approach for LCC-MMC-MTDC overhead transmission line. Int J Electr Power Energy Syst 2023;2022(144):1–10.

[3] Xue Y, Zhang X. Reactive power and AC voltage control of LCC HVDC system with controllable capacitors. IEEE Trans Power Syst 2017;32(1):100–5.

[4] Li T, Li Y, Zhu Y. DC fault current approximation and fault clearing methods for hybrid LCC-VSC HVDC networks. Int J Electr Power Energy Syst 2022;143 (108467):1–18.

[5] G. Tang, X. Luo, X. Wei. Multi-terminal HVDC and DC-grid technology. *Proceedings of the CSEE.* 2013; 33(10): 8-17.

[6] Yang D, Cheng H, Yao L, Zeng P. Research review on AC/DC hybrid system with multi-terminal HVDC. Power System Technology 2015;39(8):2201–9.

[7] Xue Y, Xu Z, Tu Q. Modulation and control for a new hybrid cascaded multilevel converter with DC blocking capability. IEEE Trans Power Del 2012;27(4):2227–37.

[8] H. Xie, C. Fu, S. Li, Y. Mei, J. Zhang, G, Xu. System Stability Characteristic Analysis on DC Line Fault Recovery and Converter Station Online Disconnection of KLL MTDC. *Southern Power System Technology.* 2021; 15(6): 654-662.

[9] Huang Q, Zhou G, Wei X. A non-unit line protection scheme for MMC-based multi-terminal HVDC grid. Int J Electr Power Energy Syst 2019;2019(107):1–9.

[10] Sneath J, Rajapakse AD. Fault detection and interruption in an earthed HVDC grid using ROCOV and hybrid DC breakers. IEEE Trans Power Del 2016;31(3):973–81.

[11] Li B, Li Y, He J, Wen W. A novel single-ended transient-voltage based protection strategy for flexible DC grid. IEEE Trans Power Del 2019;34(5):1925–37.

[12] J. Wang, C. Fu, M. Hu, D. Zhang, H. Han. Discussion on the protection in parallel-type multi-terminal HVDC systems. *Proceedings of the CSEE.* 2014; 34(28): 4923-4931.

[13] Sun G, Shi B, Zhao Y, Li S. Research on the fault location method and protection configuration strategy of MMC based DC distribution grid. Power System Protection and Control 2015;43(22):127–33.

[14] Kong F, Hao Z, Zhang S, Zhang B. Development of a novel protection device for bipolar HVDC transmission lines. IEEE Trans Power Del 2014;29(5):2270–8.

[15] X. Yu, L. Xiao. Fast Fault Detection Scheme for Multi-terminal MMC-HVDC Based on Novel Fault Directional Criterion. *Proceedings of the CSEE.* 2021; 41(24): 8437-8446.

[16] Cao R, Li Y, Xu S, Huang W, Li M, Guo Z. Research on protection configuration and coordination of UHV hybrid multi terminal DC line. Southern Power System Technology 2018;12(11):52–8.

[17] Zhang C, Song G, Dong X. Non-Unit Ultra-High-Speed DC Line Protection Method for HVDC Grids Using First Peak Time of Voltage. IEEE Trans Power Del 2021;36 (3):2825–38.

[18] Zhang C, Huang J, Song G, Dong X. Non-Unit Ultra-High-Speed Line Protection for Multi-Terminal Hybrid LCC/MMC HVDC System and Its Application Research. IEEE Trans Power Del 2021;36(5):1683–93.

[19] Zheng Y, He J, Li B. Research on DC Protection Strategy in Multi-Terminal Hybrid HVDC System. Engineering 2021;7:1064–75.

[20] Zhang Y, Tai N, Xu B. Fault Analysis and Traveling-Wave Protection Scheme for Bipolar HVDC Lines. IEEE Trans Power Del 2012;27(3):1583–91.

[21] Xu M, Cai Z, Li X. Analysis of line faults on HVDC transmission system considering frequency-dependent parameters and HVDC control. Automation of Electric Power Systems 2015;39(11):37–44.

[22] C. Zhang, G. Song, X. Dong, J. Huang. Application Research on Fast Line Protection and Adaptive Restarting Methods for Multi-terminal Hybrid LCC/MMC HVDC Transmission Lines. *Proceedings of the CSEE.* 2021; 41(11): 3873-3884.

[23] Kontos E, Pinto RT, Bauer P. Control and Protection of VSC-Based Multi-Terminal DC Networks. Lambert Academic Publishing 2013:78–83.